




# Proteomic and Transcriptomic Analysis of *Microviridae* $\varphi$ X174 Infection Reveals Broad Upregulation of Host *Escherichia coli* Membrane Damage and Heat Shock Responses

Bradley W. Wright,<sup>a</sup> Dominic Y. Logel,<sup>a</sup> Mehdi Mirzai,<sup>a,b</sup> Dana Pascovici,<sup>b</sup> Mark P. Molloy,<sup>a,b,c</sup>  Paul R. Jäschke<sup>a</sup>

<sup>a</sup>Department of Molecular Sciences, Macquarie University, Sydney, NSW, Australia

<sup>b</sup>Australian Proteome Analysis Facility (APAF), Macquarie University, Sydney, NSW, Australia

<sup>c</sup>Kolling Institute, Northern Clinical School, The University of Sydney, Sydney, NSW, Australia

Mark P. Molloy and Paul R. Jäschke are co-senior authors.

**ABSTRACT** Measuring host-bacteriophage dynamics is an important approach to understanding bacterial survival functions and responses to infection. The model *Microviridae* bacteriophage  $\varphi$ X174 is endemic to the human gut and has been studied for over 70 years, but the host response to infection has never been investigated in detail. To address this gap in our understanding of this important interaction within our microbiome, we have measured host *Escherichia coli* C proteomic and transcriptomic response to  $\varphi$ X174 infection. We used mass spectrometry and RNA sequencing (RNA-seq) to identify and quantify all 11  $\varphi$ X174 proteins and over 1,700 *E. coli* proteins, enabling us to comprehensively map host pathways involved in  $\varphi$ X174 infection. Most notably, we see significant host responses centered on membrane damage and remodeling, cellular chaperone and translocon activity, and lipoprotein processing, which we speculate is due to the peptidoglycan-disruptive effects of the  $\varphi$ X174 lysis protein E on MraY activity. We also observe the massive upregulation of small heat shock proteins lbpA/B, along with other heat shock pathway chaperones, and speculate on how the specific characteristics of holdase protein activity may be beneficial for viral infections. Together, this study enables us to begin to understand the proteomic and transcriptomic host responses of *E. coli* to *Microviridae* infections and contributes insights to the activities of this important model host-phage interaction.

**IMPORTANCE** A major part of the healthy human gut microbiome is the *Microviridae* bacteriophage, exemplified by the model  $\varphi$ X174 phage, and their *E. coli* hosts. Although much has been learned from studying  $\varphi$ X174 over the last half-century, until this work, the *E. coli* host response to infection has never been investigated in detail. We reveal the proteomic and transcriptomic pathways differentially regulated during the  $\varphi$ X174 infection cycle and uncover the details of a coordinated cellular response to membrane damage that results in increased lipoprotein processing and membrane trafficking, likely due to the phage antibiotic-like lysis protein. We also reveal that small heat shock proteins lbpA/B are massively upregulated during infection and that these holdase chaperones are highly conserved across the domains of life, indicating that reliance on them is likely widespread across viruses.

**KEYWORDS** bacteriophage, chaperone, gut microbiome, lipoprotein, mass spectrometry, RNA-seq, small heat shock proteins, sHSP, chaperones, microbiome

Successful phage reproduction relies on suppression and evasion of host defense responses (1) and, to various extents, requisitioning host machinery (2). Temporal

**Citation** Wright BW, Logel DY, Mirzai M, Pascovici D, Molloy MP, Jäschke PR. 2021. Proteomic and transcriptomic analysis of *Microviridae*  $\varphi$ X174 infection reveals broad upregulation of host *Escherichia coli* membrane damage and heat shock responses. *mSystems* 6:e00046-21. <https://doi.org/10.1128/mSystems.00046-21>.

**Editor** Seth Bordenstein, Vanderbilt University

**Copyright** © 2021 Wright et al. This is an open-access article distributed under the terms of the [Creative Commons Attribution 4.0 International license](https://creativecommons.org/licenses/by/4.0/).

Address correspondence to Paul R. Jäschke, paul.jaschke@mq.edu.au.

**Received** 12 January 2021

**Accepted** 8 April 2021

**Published** 11 May 2021

infection studies employing the use of transcriptomics (3, 4) and proteomics (5–11) have revealed insights into the establishment of infection and utilization of host machinery. In particular, the use of modern mass spectrometry workflows and instruments to identify and quantify thousands of proteins is an invaluable tool for the study of complex biological systems especially when paired with complementary RNA-sequencing (RNA-seq) methods. Currently, most phage-host interactions, even of model systems, have not yet been characterized using these methods.

Bacteriophage  $\phi$ X174 is a member of the family *Microviridae*, which make up a group of small icosahedral viruses encoded by a single-stranded DNA genome. The small 5,386-nucleotide genome of  $\phi$ X174 containing genes encoding 11 proteins makes it a tractable target for proteomic and transcriptomic studies (12, 13). *Microviridae* have been used as model systems for DNA sequencing, genome engineering (14, 15), evolution (16), icosahedral virus packaging (17, 18), and novel virus infection mechanisms (19, 20). Furthermore,  $\phi$ X174 and other *Microviridae* are universal members of the human gut microbiome (21, 22), preying on *Escherichia coli* hosts, although their precise role is not well understood.

In this investigation, we applied modern proteomics and complementary transcriptomics to map for the first time the temporal response of *E. coli* NCTC122 (C122) to phage  $\phi$ X174 infection. Our detailed measurements of protein and RNA revealed the heat shock chaperone network is selectively upregulated during infection, along with many proteins involved in membrane repair and remodeling and membrane transporters. Most notably, we observed massive upregulation of small heat shock proteins IbpA and IbpB at both the protein and RNA level. This work lays the foundation for further studies of *Microviridae* infections and their interplay within a range of more natural host strains.

## RESULTS

**$\phi$ X174 infection results in moderate changes to the host proteome and transcriptome just prior to lysis.** To measure the host response to  $\phi$ X174 infection, we first used a mass spectrometry proteomic workflow to compare biological triplicates of  $\phi$ X174-infected *E. coli* C122 and mock-infected cells at five time points (0, 15, 30, 60, and 75 min postinfection) designed to maximize coverage across the entire period leading up to and just following the onset of lysis. We found no differences between the host proteome expression and mock infections until 60 and 75 min, corresponding to the point at which we observed reduction in the rate of  $A_{600}$  increase characteristic of the beginning of lysis (see Fig. S1A in the supplemental material). Mass spectrometry analysis identified 2,173 host proteins (Data Set S1), representing  $\sim$ 57% of the *E. coli* C122 proteome database. Of the identified proteins, we measured the expression of 1,752 host proteins across all time points and replicates as well as all 11  $\phi$ X174 proteins. For these proteins, due to the different physicochemical properties of the peptides and the acquisition strategy used (23), we were limited to relative quantitation expressed as fold change (FC), which was calculated by dividing normalized area under the curve intensity measurements from condition 1 by condition 2.

To further validate our proteomics work, we also measured the transcriptional response of the host at 60 min. RNA sequencing mapped reads to 85% of *E. coli* protein-encoding genes and 100% of  $\phi$ X174 genes. Furthermore, during infection, phage-specific reads accounted for 18% of the total mapped reads.

During late infection we measured at the protein level 255 upregulated and 54 downregulated proteins (Fig. 1A; Data Set S1), while at the RNA level 203 genes were found to be upregulated and 325 genes were downregulated (Fig. 1B; Fig. S2). The *ibpA* and *ibpB* small heat shock proteins, which had FCs of +8.7/+27.1 and +15.6/+38.6 at the protein/RNA levels, respectively, were similar in magnitude and significance to the  $\phi$ X174 proteins (Fig. 1C). Notably, we did not observe any significant changes to small RNAs within *E. coli* C122 due to  $\phi$ X174 infection (Data Set S2).

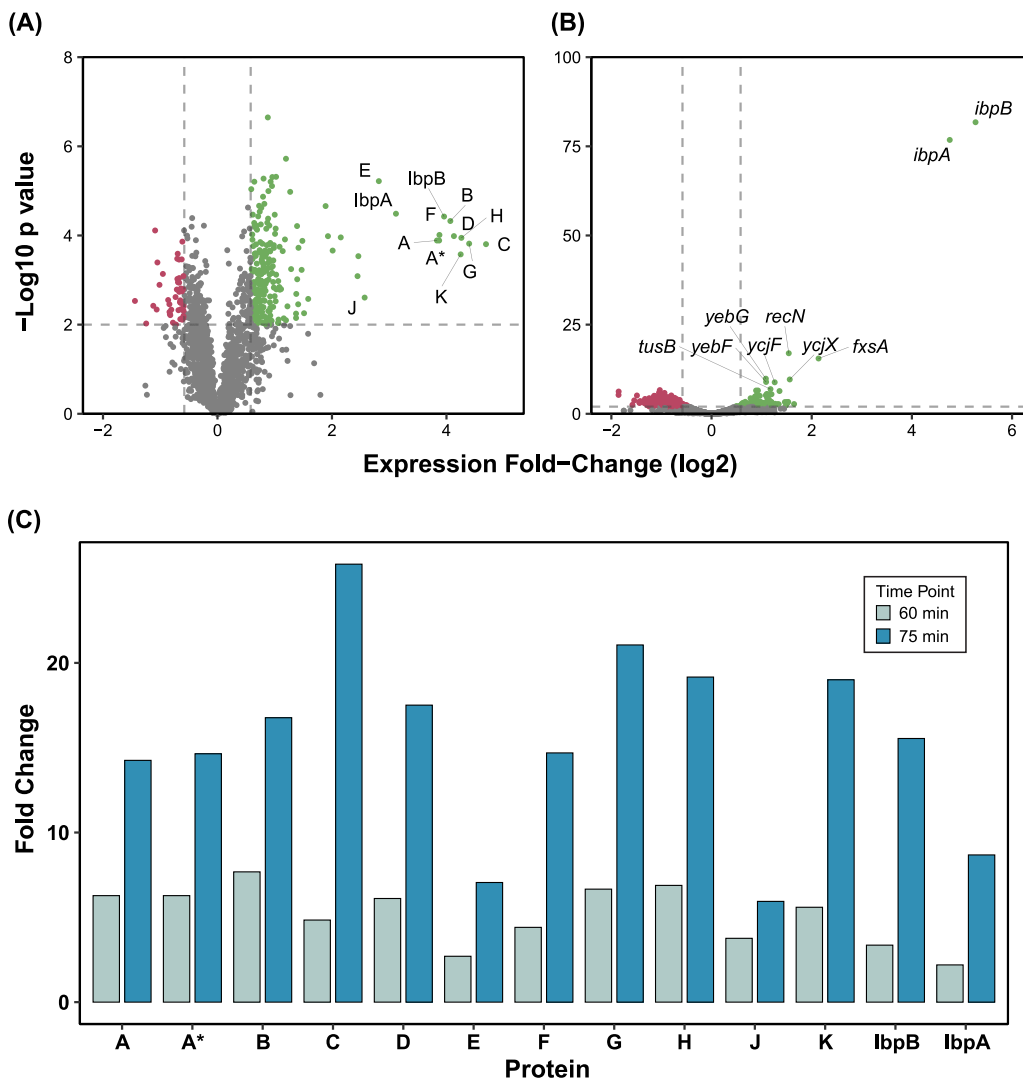


**FIG 1** A moderate number of *E. coli* C122 genes are differentially regulated during late  $\phi$ X174 infection, with *lbpAB* upregulation equal to  $\phi$ X174 phage genes. (A) Quantified proteins. FC  $\pm$ 1.5 and *P* value <0.025 significance threshold. (B) Quantified RNA. FC  $\pm$ 1.5 and *P* value cutoff <0.05 significance threshold. (C) Fold changes for  $\phi$ X174 proteins labeled A to K and host *E. coli* proteins *lbpA* and *lbpB* at 60 min and 75 min postinfection. Fold change reflects the ratio of quantified values of infected to mock samples.

**Host engages in significant membrane protein upregulation and metabolic protein downregulation during infection.** To define the broader biological impacts of  $\phi$ X174 infection, we assigned all 1,752 quantified host proteins, 11  $\phi$ X174 proteins, and 528 differentially expressed RNA transcripts to their respective clusters of orthologous groupings (COG) using eggNOGMapper (24).

The results of this analysis showed no proteomic sample preparation enrichment bias as the “Annotated C122” and “Quantified Proteins” annotated biological function category COG distributions were comparable (Fig. 2). We then partitioned the 309 significantly differentially regulated proteins at 75 min postinfection into those that were upregulated (“Up-Regulated,” *n* = 255) and those that were downregulated (“Down-Regulated,” *n* = 54). We found that all proteins annotated with COG categories M (cell wall/membrane/envelope biogenesis) and O (posttranslational modification, protein turnover, chaperones) were upregulated during infection (Fig. 2). These category enrichments indicate there may be a host response mediating significant membrane restructuring or poor translocation of membrane-bound proteins leading to their accumulation in the cytoplasm. Within the group of 54 downregulated proteins, we found

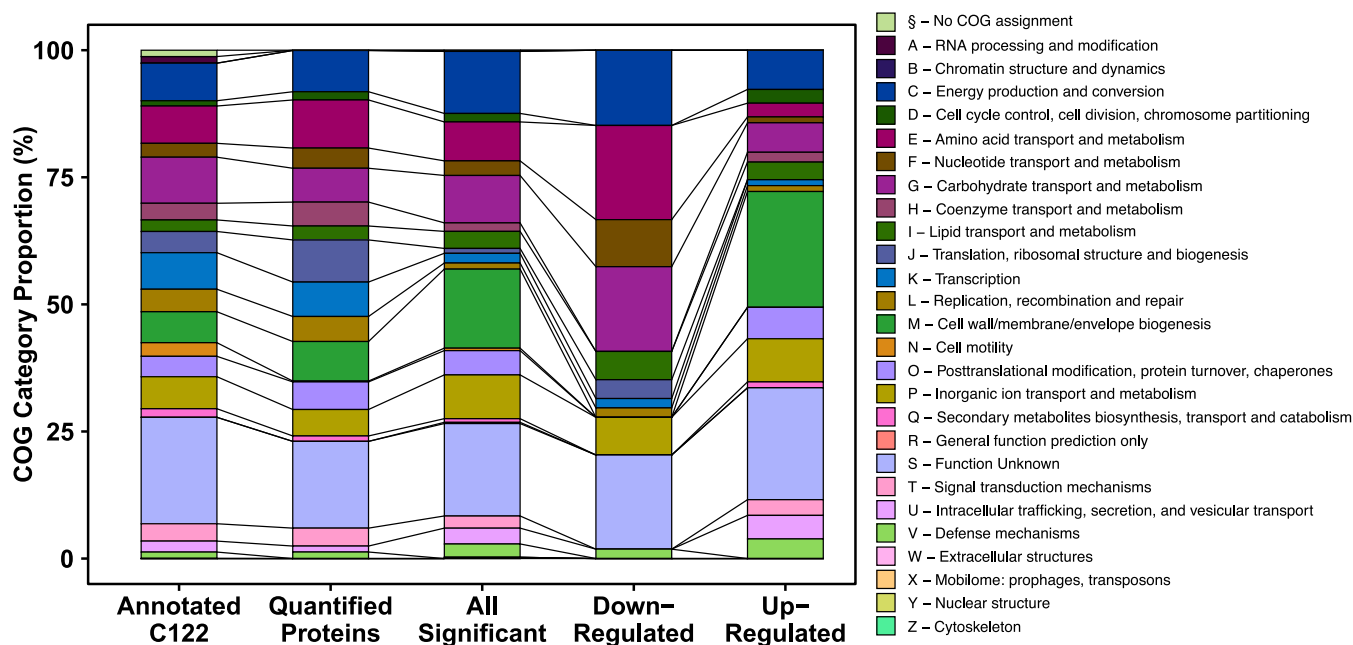


**FIG 2** Clusters of orthologous groups (COG) distributions of measured *E. coli* C122 proteins. Annotated C122, 3,666 annotated proteins; Quantified Proteins, 1,752 proteins quantified across all conditions; All Significant, nonredundant list of 399 significantly differentially regulated proteins across all time points and samples; Down-Regulated, 54 significantly downregulated proteins from 75 min postinfection; Up-Regulated, 255 significantly upregulated proteins from 75 min postinfection. COGs were assigned to C122 genes using the eggNOG-Mapper (24).

the majority of these proteins (~59%) were in COG categories representative of energy and metabolism (C, E, F, and G) (Fig. 2).

Using the PANTHER overrepresentation test (25), we mapped these proteins according to their GO cellular component annotations. We found that of the upregulated proteins, 167 (65%) could be mapped to a cellular component, of which 21 (13%) were localized to the cytoplasm. These included small heat shock proteins lbpA and lbpB. Similarly, 39 (72%) of the downregulated proteins could be mapped to their cellular component, and 24 (62%) of these were mapped to the cytoplasm.

Corresponding with the proteomic findings, the transcriptomics showed COG category enrichment for inorganic ion transport and metabolism (P), amino acid transport and metabolism (E), and energy production and conversion (C) (Fig. S3). Additionally, the transcriptomics showed enrichment for the COG categories cell motility (N) and intracellular trafficking, secretion, and vesicular transport (U). PANTHER overrepresentation testing for GO cellular component terms showed significant enrichment within upregulated genes for the pilus (6.7-fold) and the integral component of the membrane (1.6-fold). The downregulated genes were enriched for the iron-sulfur cluster assembly complex (16.2-fold), the proton-transporting ATP synthase complex, catalytic core F(1) (13.5-fold), and the plasma membrane respiratory chain complex I (11.2-fold) (Fig. S4). All of these enriched cellular components are localized within the bacterial membrane. Membrane component enrichment was reflected in the differentially expressed genes more broadly as well, as gene products destined for the membrane accounted for 42% and 24% of the up- and downregulated data sets, respectively.

To understand the interaction of  $\varphi$ X174 protein expression and host responses to infection, we performed comparative analyses using an UpSet plot, which is a tool to visualize and group shared elements within intersecting data sets (26). We used the UpSet visualization to identify the conditions and samples in which significantly differentially regulated proteins are shared. This analysis revealed that the 60-min-postinfection samples (60C and 60P) shared 12 differentially expressed proteins with the 75-min-postinfection samples (75C and 75P): two host proteins (lbpA and lbpB), and all  $\varphi$ X174 proteins except C protein (Fig. 3A; Data Set S1).

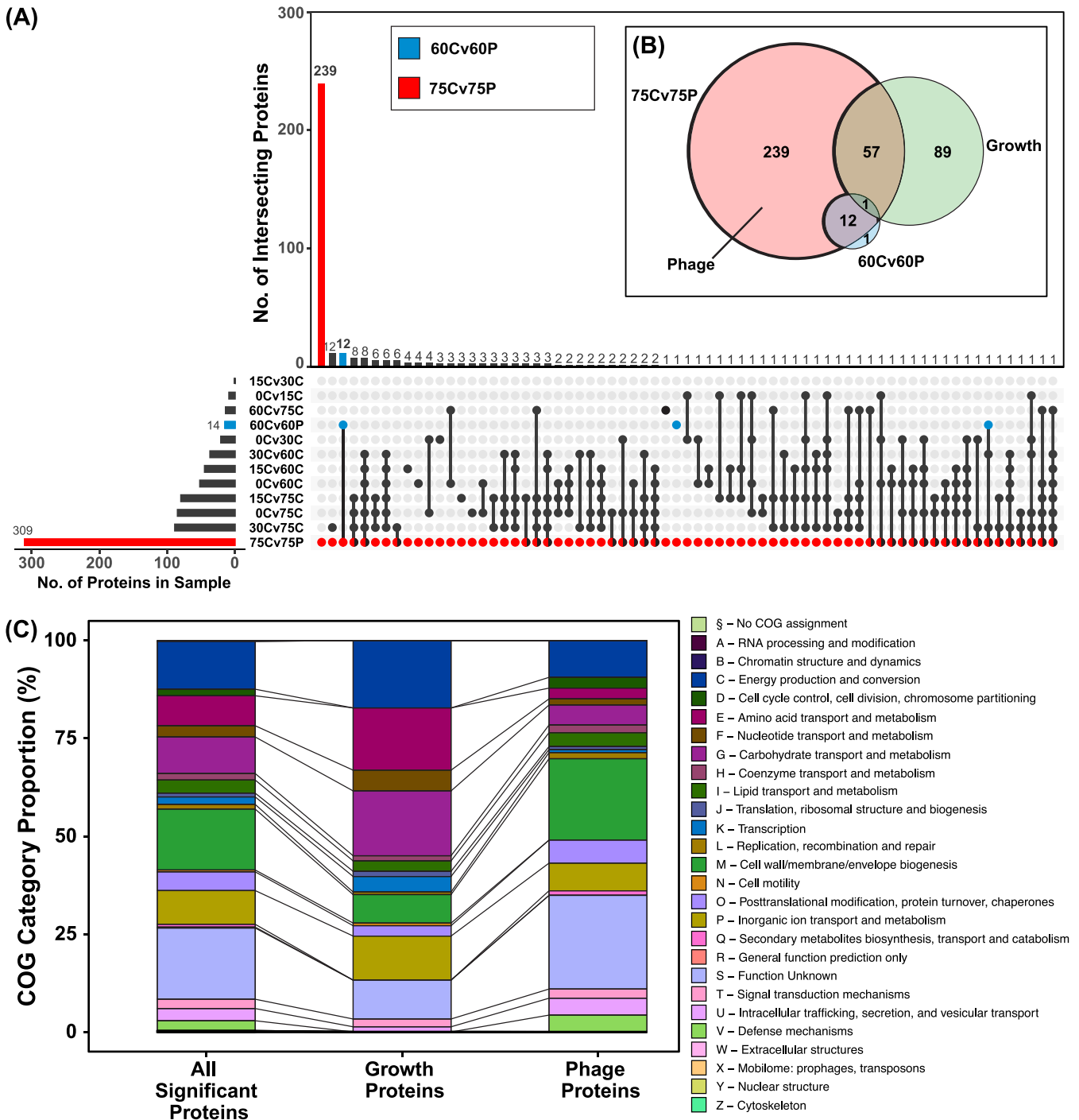


**FIG 3** Sets of significantly differentially regulated proteins due to cellular growth and  $\phi$ X174 infection and their functional groupings. (A) UpSet visualization of sample groups analyzed by proteomics. Each set represents the group of significantly regulated proteins ( $FC \pm 1.5$ ,  $P$  value  $< 0.025$ ) extracted from comparative analyses. For example, 75Cv75P (red) is the group of significant proteins passing our stated cutoff thresholds when the 75-min mock-infected (75C) group is compared to the 75-min  $\phi$ X174-infected (75P) group. This plot allows visualization of redundant proteins found differentially regulated across multiple groups and, more importantly, facilitates the partitioning out of significant proteins relevant only to  $\phi$ X174 infection. Nonredundant sample size = 399 proteins. (B) Euler plot showing relationships between Phage, Growth, 60Cv60P, and 75Cv75P protein sets. (C) Clusters of orthologous groups (COG) categories of the Growth and Phage protein sets compared to 399 significant proteins (“All Significant Proteins”). See Data Set S1. COGs were assigned to C122 genes using the eggNOG-Mapper (24).

In contrast to the 60-min samples, the 75-min-postinfection samples showed large-scale changes to the host proteome, with 309 differentially regulated proteins including all 11 phage proteins and the same two host proteins, lbpA and lbpB, seen at 60 min (Fig. 3A). Within this group of 309 proteins, we wanted to identify proteins that

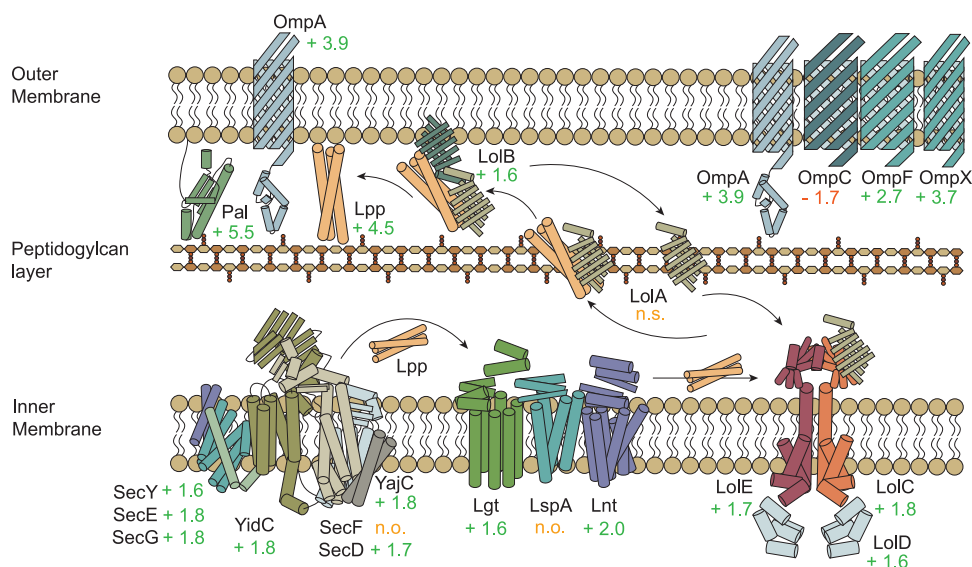


**FIG 4** *E. coli* C122 upregulates membrane-stabilizing and -anchoring proteins Lpp, OmpA, and Pal during  $\phi$ X174 infection. Upregulation of the membrane lipoprotein maturation and transportation pathway. Depicted are nascent lipoproteins translocating across the inner membrane through the Sec pathway, followed by processing, and Lol pathway-mediated export to the outer membrane. Outer membrane proteins are depicted, including OmpA, which has its peptidoglycan-anchoring role highlighted along with Lpp and Pal. Values indicate protein fold change during infection (75P/75C protein samples), n.o., protein not observed; n.s., protein observed but not significantly altered in abundance between conditions.

were strictly impacted due to the phage infection and not cellular growth, which was also occurring during the phage infection. To identify proteins that changed in expression due to cellular growth alone, we compared all permutations of mock-infected time points and identified 147 proteins that were differentially regulated due to cell growth. We called this group Growth (Fig. 3B). Comparing the Growth proteins to the 309 proteins differentially regulated at 75 min postinfection revealed a set of 58 proteins differentially regulated due to both Growth and  $\phi$ X174 infection (Fig. 3B). Removing these 58 proteins along with the 12 proteins shared with the 60-min-postinfection sample gave a set of 239 proteins differentially regulated due solely to phage infection. We called this group Phage (Fig. 3B).

Examining the biological functions enriched within the Growth protein set revealed proteins involved in metabolic activity such as energy production and conversion (C) and amino acid (E) and carbohydrate (G) transport and metabolism (Fig. 3C). In contrast, Phage proteins were enriched for a distinct set of categories: cell wall/membrane/envelope biogenesis (M); intracellular trafficking, secretion, and vesicular transport (U); and defense mechanisms (V) (Fig. 3C).

**Disruption to peptidoglycan synthesis and upregulation of membrane-tethering lipoproteins associated with  $\phi$ X174 protein E expression.** Looking deeper into the COG category M (cell wall/membrane/envelope biogenesis), we found proteins from the outer membrane lipoprotein maturation and transportation pathway were significantly upregulated. Typically, a protein is translocated across the inner membrane from the cytoplasm by the Sec pathway or via the twin-arginine translocation (TAT) pathway. We did not observe differential regulation of the TAT pathway but did see the upregulation of all components of the cytoplasmic membrane complex of the Sec pathway (SecYEG, FCs +1.6, +1.8, and +1.8, respectively) and the accessory protein YidC (FC +1.8) (27) (Fig. 4). PANTHER overrepresentation analysis of proteins identified as upregulated from the Phage protein set (Data Set S1) highlighted that the cell envelope Sec protein transport complex is significantly overrepresented ( $P$  value < 0.0002) during infection. This complex facilitates the translocation of nascent unfolded proteins into the periplasm in an ATP-dependent fashion (28). We did not

identify differential expression of SecA, an ATPase that interacts with SecYEG and SecB (29), nor the significant differential expression of SecB itself. SecF was not observed, but its binding partner, SecD, was significantly upregulated (FC +1.7). YajC also interacts with SecDF and we saw it significantly upregulated (FC +1.8) to a similar magnitude during  $\varphi$ X174 infection (Fig. 4).

After nascent lipoproteins are translocated through the inner membrane via the Sec pathway machinery, a diacylglycerol group is added to the protein by the inner membrane diacylglycerol transferase protein Lgt (30). We observed the significant upregulation of Lgt in the phage-infected samples (FC +1.6) as well as the Lnt protein that subsequently performs N-terminal acylation (FC +2.0) (30), but we did not observe signal peptide cleaving protein LspA (Fig. 4). The ATP-driven LolCDE inner membrane complex (FCs +1.8, +1.6, and +1.7, respectively) releases lipoproteins to the periplasmic chaperone protein LolA (expression not significantly changed) (31). From there, LolA facilitates the lipoprotein's transfer to the outer membrane receptor LolB (FC +1.6), which mediates their integration into the outer membrane (32) (Fig. 4).

The upregulation of the lipoprotein processing and trafficking machinery was in concordance with the upregulation of the major outer membrane lipoprotein (Lpp) in the Phage protein set (FC +4.5) (Fig. 4). Lpp tethers the outer membrane to the peptidoglycan layer through a covalent linkage, facilitating structural integrity and maintenance of cell shape (33). Lpp attachment to the outer membrane is dependent on LolB (FC +1.6), which, if depleted, is detrimental to the cell due to Lpp mislocalization (34). Similar to Lpp, we saw upregulation of OmpA and Pal (FCs +3.9 and +5.5, respectively), which also function in maintenance of cell membrane integrity and act through noncovalent interactions connecting the outer membrane and peptidoglycan layers (35, 36) (Fig. 4). This result suggests the cell, during  $\varphi$ X174 infection, was experiencing envelope integrity problems, possibly of the peptidoglycan layer, resulting in the upregulation of these membrane-anchoring proteins.

Previous work has demonstrated that phage lysis protein E acts to directly disrupt the activity of integral inner membrane protein MraY (37–39). MraY catalyzes the first membrane-associated step of peptidoglycan biosynthesis (40), and interruption of MraY function by protein E is believed to result in the loss of envelope integrity through synthesis inhibition (38). While the complete mechanism is yet to be resolved, lysis protein E is expressed at increasing amounts throughout the infection cycle and the lytic response is coupled to the cell growth rate and nutritional state (41). Furthermore, protein E expression seems to be associated with failed septation (42, 43).

We first observed protein E at 60 min, and by 75 min, expression had more than doubled (Fig. 1C). At 75 min we saw upregulation of MraY (FC +1.8) and all observed downstream inner membrane proteins in this pathway, MurG (FC +1.7) and FtsW (FC +1.7), although we saw no upregulation of the cytoplasmic components of the peptidoglycan biosynthetic pathway that lie immediately upstream of the MraY protein (Fig. 5).

In contrast to the extensive proteome-level response, only 16 differentially expressed RNA transcripts were attributed to COG category M. Within this grouping, only two genes, *murl* and *yjdB*, are involved in lipopolysaccharide biosynthesis. *murl*, which is responsible for lipopolysaccharide core region biosynthesis by catalyzing the racemization of L-glutamate to D-glutamate (44), was downregulated (FC -1.5), while *eptA*, which catalyzes the addition of phosphoethanolamine to the lipid A glucosamine disaccharide (45) was upregulated (FC +1.6).

**Transcriptomics identifies significant upregulation of the PSP stress response operon, revealing additional cellular response to membrane damage.** A major transcriptional response of *E. coli* C122 to  $\varphi$ X174 infection was the upregulation of gene products responsible for maintaining envelope integrity and the proton motive force. This was primarily seen through the upregulation of multiple components of the phage shock protein (PSP) response whereby *pspB* (FC +1.7), *pspC* (FC +1.7), and *pspD* (FC +1.8) in the *pspABCDE* operon, and *pspG* (FC +1.8), were upregulated. Collectively, these genes encode protein products responsible for the binding of PspA to damaged

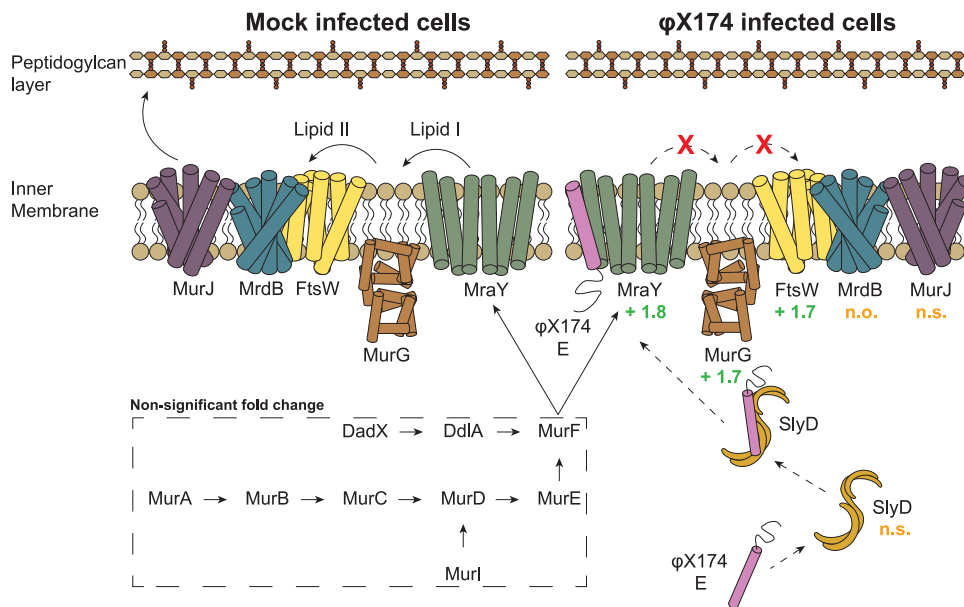


**FIG 5** Selective upregulation of the membrane-bound steps of peptidoglycan synthesis observed during infection. Membrane-bound and cytoplasmic proteins involved in peptidoglycan synthesis shown along with  $\phi$ X174 protein E, which inhibits MrdA. Values indicate protein fold change during infection (75P/75C protein samples); n.o., protein not observed; n.s., protein observed but not significantly altered in abundance between conditions.

membranes. At the proteome level, significant upregulation was observed only for PspB (FC +2.1), while PspE was downregulated, and no change was observed for PspA, PspC, and PspF. Two other genes, *ycjF* and *ycjX*, associated with the PSP response in some species (46), were also upregulated at both the transcriptional and protein levels (RNA FCs +2.4 and +3.0 [Fig. S2B]; protein FCs +2.6 and +1.7, respectively).

One of the most upregulated genes during infection was *fxsA* (FC +4.4), which was not identified in the proteomic analysis. Its only ascribed function is to competitively sequester PifA in the cytoplasmic membrane, preventing PifA from performing its host suicide mechanism, known as F exclusion. F exclusion disrupts the bacteriophage T7 life cycle by arresting all viral and cellular processes upon PifA interaction with T7 products gp1.2 and gp10A (47, 48). No annotated version of *pifA* is in the available C122 genomes, and it is normally found on the F plasmid, which was not present in the cells in this work.

**$\phi$ X174 infection significantly alters *E. coli* metabolic gene expression.** To understand the effects of the phage infection on the 58 proteins detected in both Growth and Phage sets (Fig. 6D), we classified them based on their three distinct patterns of differential regulation (Fig. 6A to C). The first set showed  $\phi$ X174 infection dampening protein expression across 17 genes (Fig. 6A). PANTHER GO biological process analysis of this list found enrichment in proteins involved in the tricarboxylic acid cycle (4 proteins,  $P$  value =  $5.79E-06$ ), indicative of a disruption to overall metabolic activity during phage infection. The second group of genes showed increased expression in the Phage protein set (Fig. 6B). PANTHER GO molecular function analysis on these 14 proteins found enrichment for transporter activity (9 proteins,  $P$  value =  $3.59E-06$ ) or, more specifically, carboxylic acid transmembrane transporter activity (5 proteins,  $P$  value =  $8.50E-06$ ). This is reflective of COG distributions of the entire 58 proteins (Fig. 6E), where we see the majority of the highlighted categories being trafficking or transporter groups. The third case showed inverse protein expression pattern between Growth and Phage sets (Fig. 6C), which is especially intriguing as it would indicate these proteins are particularly important to phage infection. A PANTHER GO biological process or molecular function analysis of these 28 genes revealed no significant enrichment. However, 15 of the 28 proteins are located in the cell envelope ( $P$



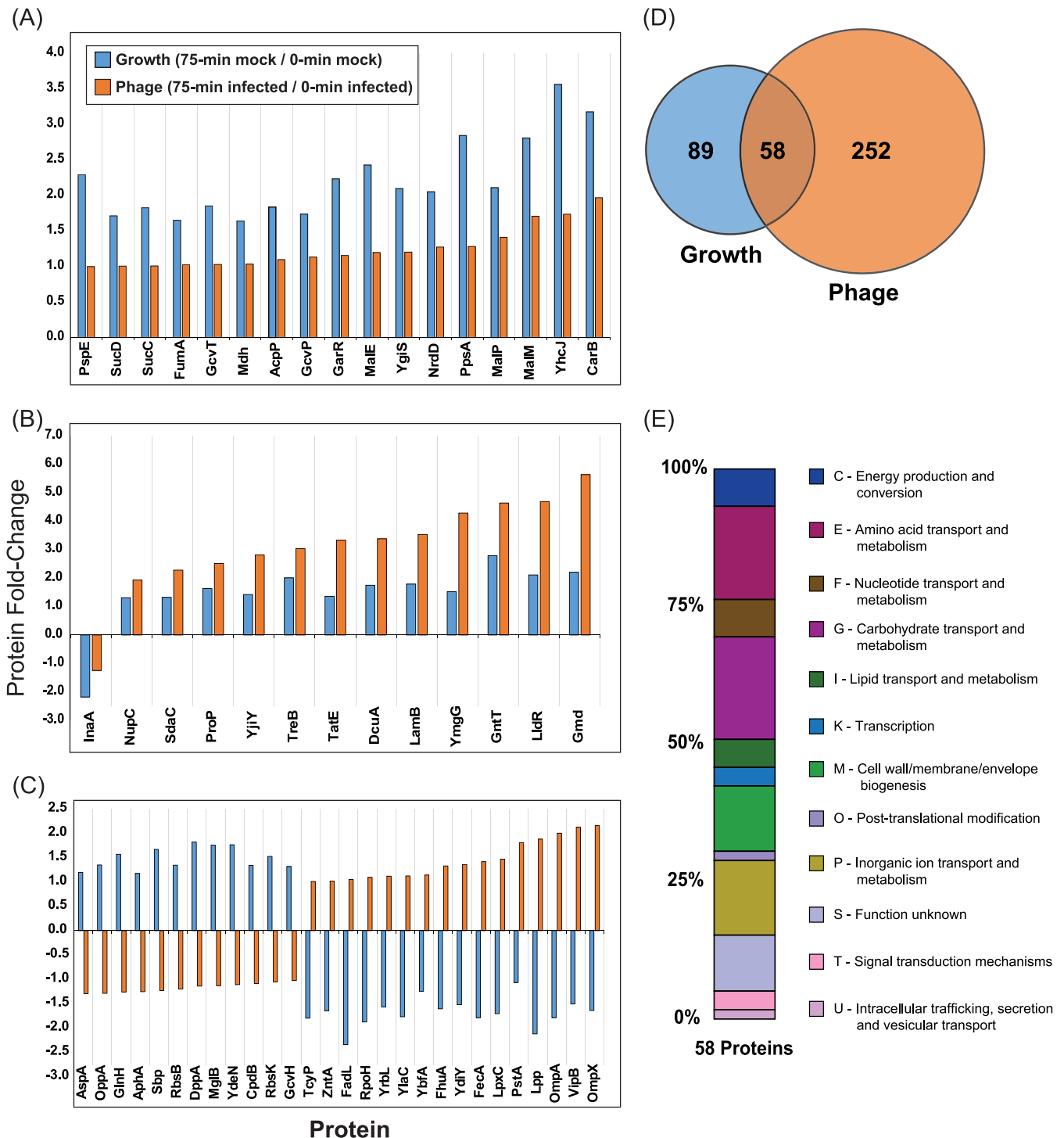


**FIG 6** Differential expression patterns of the 58 *E. coli* C122 proteins shared by Growth and Phage sets. (A to C) Subset of the 58 host proteins where  $\phi$ X174 infection reduces (A), increases (B), or inverts (C) expression. (D) Euler plot of all significantly differentially expressed proteins within the Growth and Phage sets. (E) Clusters of orthologous groups (COG) functional categories used to represent major biological functions and their percent (%) distribution across different groupings for the 58 shared proteins. COGs were assigned to C122 genes using the eggNOG-Mapper (24).

value =  $2.82E-11$ ), indicating significant and likely diverse transporter functions from this group of proteins. Of particular interest are aforementioned proteins Lpp and OmpA, as well as OmpA structural homolog OmpX (FC +3.7) (Fig. 4) (49), all of which were found to have large fold change inductions during phage infection but were downregulated during mock infection (Fig. 6C).

Interestingly, OmpA was recently identified as a competitive binder of the lipoprotein RcsF (49), which we also identified as significantly upregulated during phage infection (FC +1.6). RcsF is a positive regulator of the Rcs stress response (50), of which we identified the significant upregulation of Rcs components RcsD (FC +1.7) during infection.

Biological process GO term enrichments of the transcriptomics data showed broad representation of two different host functions which affected host metabolic activity when mapped to COG categories. The first of these host functions corresponded to the COG categories nucleoside transport and metabolism (F), amino acid transport and metabolism (E), and carbohydrate transport and metabolism (G). The COG categories were represented with the enriched biological functions of plasma membrane glucose import (17.9-fold, 4 genes,  $P$  value =  $4.50E-04$ ), glycine catabolic process (14.3-fold, 4 genes,  $P$  value =  $7.77E-04$ ), nucleoside transmembrane transport (11.2-fold, 5 genes,  $P$  value =  $3.59E-04$ ), and nucleobase-containing small-molecule interconversion (5.5-fold, 7 genes,  $P$  value =  $7.54E-04$ ). The second host function mapped to COG categories corresponded to energy production and conversion (C) with the enriched biological functions ATP synthesis-coupled proton transport (11.2-fold, 5 genes,  $P$  value =  $3.59E-04$ ), gluconeogenesis (7.7-fold, 6 genes,  $P$  value =  $4.24E-04$ ), and glycolytic process (6.0-fold, 7 genes,  $P$  value =  $4.81E-04$ ) (Fig. S4).

**$\phi$ X174 infection strongly activates heat shock chaperone response.** The strongest host response we observed at both the protein and RNA level was the heat shock response, led by the small heat shock proteins (sHSPs) IbpA and IbpB (Fig. 1). Our proteomics and transcriptomic data showed that they had the largest increase in expression of any host gene products (Fig. 1C). Both *ibpA* and *ibpB* are controlled by the  $\sigma^{32}$  regulon (51), and their large upregulation during  $\phi$ X174 infection is consistent with the significant increase in RpoH transcription factor  $\sigma^{32}$  (FC +2.0), along with chaperones ClpB (FC +1.7) and DnaJ (FC +1.9) (Fig. 7). Notably, only a subset of the  $\sigma^{32}$  heat shock stress response regulon was activated during  $\phi$ X174 infection, as we observed only 11 proteins and 17 transcripts belonging to this regulon differentially regulated (Fig. 7; Data Set S3). Similarly, the general stress response master regulator,  $\sigma^{38}$  (RpoS), was not differentially regulated, and only a small proportion of proteins (5%) from the genes under its control were differentially regulated during phage infection (Data Set S3).

Together, these data indicate that  $\phi$ X174 infection was not inducing a general stress response via the  $\sigma^{38}$  or  $\sigma^{32}$  regulon and that there was selective upregulation of members of the heat shock chaperone network (Fig. 7).

## DISCUSSION

In this work, we have comprehensively measured the *E. coli* C122 host response to  $\phi$ X174 infection at the proteomic and transcriptomic level, representing the first characterization of the dynamics of *Microviridae* infection at this level of detail. We identified 2,184 proteins and quantified all 11 phage proteins and 1,752 host proteins across seven time points spanning the entire infection cycle. Transcriptomics identified significant changes during infection including differential expression of 528 genes, constituting 11% of the total transcriptome, similar to other studies (52).

We found no evidence for substantial host proteome remodeling during the early stages of infection prior to 60 min (Fig. 3A), which aligns with previous work showing that  $\phi$ X174 has a minimal impact on host protein production until just prior to lysis (53). Between 60 min and 75 min, we saw 255 proteins upregulated while only 54 were downregulated, with the most strongly downregulated proteins decreasing faster than would be expected from dilution due to cell growth (see Fig. S5 in the supplemental material). It is well established that phage infection can cause drastic and broad metabolic remodeling of infected cells (11, 54, 55), which is in agreement with what we saw for both our proteomic and transcriptomic data sets.

We showed that membrane damage responses dominated the host response to  $\phi$ X174 infection (Fig. 4 and 5). We also found membrane lipoprotein maturation and

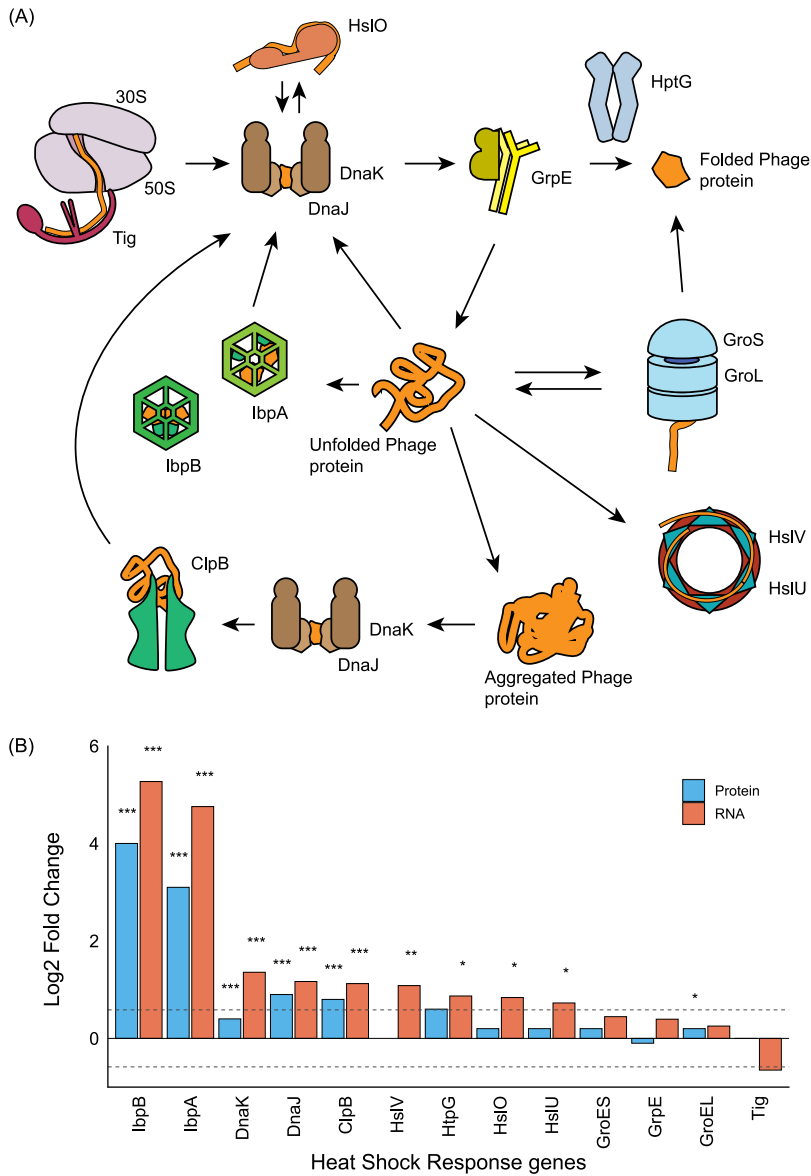


**FIG 7** Large changes to gene expression across the heat shock chaperone and protein folding pathway in *E. coli* C122 during  $\phi$ X174 infection. Proteins depicted in this pathway are transcriptionally regulated by transcription factor RpoH ( $\sigma^{32}$ ), which we saw upregulated during infection. (A) The chaperone system revealing the process controlling protein folding from synthesis to native protein state. The chaperone trigger factor (Tig) binds to the translating ribosome and the growing peptide chain. The DnaK/J chaperone proteins aid in folding by binding to hydrophobic regions of nascent proteins, preventing their misfolding and aggregation. DnaK/J may bind to HtpG to reactivate inactive protein substrates on the path to native protein fold (93). The holdase HsIO binds to unfolded protein, which is released to DnaK for folding (94). GrpE may interact with DnaK, thereby dissociating ADP and releasing the bound protein (95). Small heat shock chaperones IbpA/B bind nascent proteins, preventing their irreversible aggregation into inclusion bodies, and await the availability of folding chaperones DnaK/J and GroEL/ES. The main folding machine of the system is the GroEL/ES complex. This ATP-dependent system facilitates folding of nascent proteins within the complex's inner surface, releasing proteins in their native state. In the case of protein aggregates produced from improperly or partially folded proteins, the chaperone ClpB mediates their disaggregation for their refolding. Unfolded protein may also shuffle to the HsIUV protease/ATPase complex for proteolysis (96). (B) Differential expression of transcripts and proteins was measured at 60 and 75 min, respectively. Dashed lines indicate the  $\log_2$  fold change  $\pm 0.58$  values used as significance criteria. *P* values are shown as \*\*\* for  $\leq 0.001$ , \*\* for  $\leq 0.01$ , and \* for  $\leq 0.05$ .

transportation pathway enrichment (Fig. 4), which suggests an upregulation of this pathway in response to the host's need to traffic certain lipoproteins to the outer membrane, such as major lipoprotein (Lpp). Lpp is one of the most abundant (lipo)proteins of *E. coli* (56) and is reliant on the Lol pathway for outer membrane insertion (34). We saw Lpp downregulated during growth (FC  $-2.1$ ) and upregulated during  $\varphi$ X174 infection (FC  $+4.5$ ), thus emphasizing an infection-mediated response. Lpp has recently been shown to regulate cell shape and mechanical rigidity by tethering the outer membrane to the peptidoglycan layer (33), which leads us to suggest that during  $\varphi$ X174 infection, Lpp is upregulated to maintain the cell's envelope integrity.

The most likely model that fits our observations would have lysis protein E from  $\varphi$ X174 binding to and inhibiting MraY (37, 38) and causing a decrease in peptidoglycan synthesis which is sensed by the cell and results in upregulation of MraY and inner membrane pathway partners, MurG and FtsW (Fig. 5). The cytoplasmic components of the peptidoglycan pathway and the chaperone protein, SlyD, which stabilizes the  $\varphi$ X174 lysis protein E and is thought to promote its interaction with the inner membrane (57), are not upregulated (Fig. 5).

Secondarily, as the  $\varphi$ X174-infected *E. coli* cell continues to grow but is unable to synthesize enough peptidoglycan, the stability of the envelope becomes compromised. The cell senses this and attempts to compensate by upregulating the Lpp, OmpA, and Pal proteins (Fig. 4). OmpA also seems to have a role in maintaining envelope integrity by linking the outer membrane to the peptidoglycan layer through the noncovalent linkage of its C-terminal domain to peptidoglycan (36). In addition to this activity, OmpA has a direct interaction with peptidoglycan stress sensory protein RcsF (49), which we also saw upregulated during infection (FC  $+1.6$ ). Pal protein is also a mediator of outer membrane and peptidoglycan stability by forming a structural linkage between both layers (35).

Host membrane responses to phage infection are common and can involve responses such as induction of polysaccharide capsule biosynthesis (58) and phage shock response (55). We saw the significant upregulation of components *pspB*, *pspC*, and *pspG* and the potentially related genes *ycjX* and *ycjF* (Fig. S2), presumably in response to the loss of envelope structural integrity during the leadup to lysis. A similar induction of the phage shock response was observed with phage PRD1 infection of *E. coli* (59) and antibiotics that inhibit peptidoglycan synthesis (60).

Both proteomics and transcriptomics showed a massive upregulation of small heat shock proteins IbpA (FC  $+8.7$ ) and IbpB (FC  $+15.6$ ) and their transcripts (FC  $+27.1$  and  $+38.6$ , respectively) during infection. The IbpA/B proteins are well described, and the sHSP family is conserved across all domains of life (61). They are typically described as "holdase" proteins, as they function as chaperones binding misfolded or unfolded (nascent) proteins to prevent their irreversible aggregation within the cytosol, while they wait for available ATP-mediated folding machinery (62, 63) (Fig. 7). The large mismatch between *ibpA/B* RNA and protein fold changes in our measurements may be due to the RNA thermometer function encoded within their transcripts that ensures they are maximally translated only at elevated temperatures (64).

We speculate that the upregulation of IbpA/B proteins is a conserved nonspecific bacterial response to viral infection based upon their upregulation both during phage infection (59, 65) and during heterologous protein overexpression (66, 67). Therefore, as a result of their currently defined function (62, 63), IbpA/B upregulation in *E. coli* C122 during  $\varphi$ X174 infection is a host response to higher-than-normal levels of protein production (in this case, phage protein production), and in the absence of available protein folding machinery, irreversible protein aggregation or misfolding is prevented through the upregulation of these holdase proteins.

Phage may also benefit from the specific features of the IbpA/B function by having a queue of proteins held in a near-folded state that can be quickly folded into their final forms by HSP70 (DnaK) and HSP100 (ClpB) activity. Proteins bound by IbpA/B are

not spontaneously released and can be released only by DnaK and ClpB (64), introducing a buffering system and control point for virion assembly.

The *ibpA/B* genes have never been identified from genetic screens of host factors necessary for capsid morphogenesis, but sHSPs are encoded in the genomes of cyanophage infecting *Synechococcus* and *Prochlorococcus* groups (68, 69). Furthermore, a bacteriophage-encoded J-domain protein (Rki) has been identified in T4-related enterobacteriophage RB43 that interacts with *E. coli* J-domain-interacting chaperone protein DnaK (HSP70) and stabilizes the  $\sigma^{32}$  heat shock response (70). MS2 phage relies on DnaJ (HSP40) (71), while the HSP60 chaperones GroEL/ES are required for phage  $\lambda$ , PRD1, HK97, and T7 morphogenesis (72–74). GroEL-like proteins have also been found encoded within newly annotated bacteriophage genomes (75). In *groEL/groES* mutants, phage T4 head morphogenesis is disrupted and results in a random aggregation of phage head proteins attached to the inner membranes (76), pointing to the critical disassembling and/or folding role of the HSP chaperones in phage capsid assembly. Young et al. (1989) found that lysis sensitivity increased in *E. coli* when plasmid-encoded  $\phi$ X174 lysis protein E and heat shock genes *dnaK*, *dnaJ*, *groEL*, and *grpE* are present (77). Recently,  $\phi$ X174 has been suggested to use heat shock promoters to co-opt host responses to infection to drive its life cycle (12, 78). Therefore, together with our data, we propose that the host heat shock response and in particular IbpA/B are important components for  $\phi$ X174 replication.

## MATERIALS AND METHODS

**$\phi$ X174 infection.** Methods are composed in accordance with reference 79. Media and buffer components were from Sigma-Aldrich, unless stated otherwise. *E. coli* C122 (Public Health England NCTC122) was grown overnight at 37°C/250 rpm in phage-LB (80) and then inoculated 1/100 in fresh phage-LB and grown to mid-log phase ( $\sim 0.7$  OD<sub>600</sub>) before addition of phage (37°C/250 rpm). Wild-type  $\phi$ X174 (14) was used for all infections of *E. coli* C122 at a multiplicity of infection (MOI) of 5. Phage infection was synchronized by pelleting mid-log cultures (4,000 relative centrifugal force [RCF]/8 min) and resuspending the pellet to 1/10 of the original growth volume with cold HFB buffer (81). Starved cells were incubated at 16°C/30 min to facilitate phage attachment and to prevent DNA ejection (82). After 30 min, infection was initiated with the addition of phage-LB (37°C) to the original volume. Controls (mock infected) had the same volume of phage-LB and 10 % (vol/vol) glycerol added at mid-log phase as the phage-infected samples.

**Protein purification and tandem mass tagging (TMT) labeling.** Biological triplicates of *E. coli* C122 were grown to mid-log in a 200-ml culture volume (37°C/250 rpm) and then split into two 100-ml volumes: one to be infected with  $\phi$ X174 at an MOI of 5 and the other mock infected with an equal volume of phage-LB with 10% (vol/vol) glycerol (storage solution of  $\phi$ X174). Culture growth was synchronized with 10 ml of ice-cold HFB, and infection was initiated with 90 ml phage-LB (37°C). At 0, 15, 30, 60, and 75 min postinfection, 12 ml was removed from each culture (without replacement) and placed on ice. At the conclusion of the time course, intact cells were pelleted at 3,220 RCF/8 min. The samples were then suspended in cold 1 $\times$  phosphate-buffered saline (PBS) and washed an additional two times, discarding the supernatant. Cell pellets were stored overnight at  $-20^{\circ}\text{C}$ . Cell pellets were suspended in 500  $\mu\text{l}$  lysis buffer (100 mM Tris-HCl, 1% [vol/vol] sodium dodecyl sulfate, 8 M urea, 1 $\times$  protease inhibitor cocktail solution [Roche, Switzerland]). Reconstituted cells were lysed with a Branson Sonifier 450 ultrasonic probe with 15 pulses for 15 s at a 30% duty cycle and 30% amplitude. Samples were then pelleted at 6,000 RCF/10 min, and supernatant was moved to a new tube. Proteins were reduced at 37°C/1 h in 10 mM dithiothreitol, followed by alkylation with 30 mM iodoacetamide for 1 h in the dark. Residual iodoacetamide was quenched with an equal molarity of dithiothreitol.

Proteins were precipitated by addition of 2 ml methanol, 0.5 ml of chloroform, and 2 ml of water (all ice cold). Samples were pelleted at 5,000 RCF/10 min, and protein pellet was removed, washed with additional methanol, and dried. Protein pellets were solubilized with 100 mM Tris-HCl/8 M urea. Solutions were pelleted at 12,000 RCF/10 min, and supernatant was collected in a new tube. Samples were diluted to a urea concentration of 1.6 M through addition of 100 mM Tris-HCl, followed by protein quantitation (Pierce bicinchoninic acid [BCA] protein assay kit; ThermoFisher Scientific). One hundred fifty micrograms of protein from each sample was digested overnight/37°C with 1.5  $\mu\text{g}$  trypsin (Promega), followed by addition of a further 1.5  $\mu\text{g}$  of trypsin and digestion for an additional 4 h. Peptides were acidified with formic acid at 1% (vol/vol) and then C<sub>18</sub> stage-tip purified (83). Peptide samples were dried down using vacuum centrifugation, followed by resuspension in 200 mM HEPES buffer (pH 8.8, adjusted with NaOH). Peptides were quantified (Micro BCA protein assay kit; ThermoFisher Scientific), and 35  $\mu\text{g}$  peptide from each sample was brought up to 140  $\mu\text{l}$  using HEPES buffer. Normalization controls were produced through pooling mock-infected samples (3  $\mu\text{g}$  of peptide per mock-infected sample), designated N.C., and infected samples (3  $\mu\text{g}$  of peptide per infected sample), designated N.P.

Chemical labeling of peptide samples was performed using the TMT 10-plex isobaric label reagent set (ThermoFisher Scientific, USA). An 0.2-mg amount of TMT tag was used to label each sample (see

Table S1 in the supplemental material). Note that 128C tag was reserved for N.C. An 11.25- $\mu\text{g}$  amount of N.C. was labeled per channel. Similarly, 131 tag was reserved for N.P. A 5.375- $\mu\text{g}$  amount of N.P. was labeled per channel. After labeling, 8  $\mu\text{l}$  of 5% (vol/vol) hydroxylamine was added to each sample to quench residual tags. Lastly, samples were combined across channels, dried down using vacuum centrifugation, and then purified as described previously (83).

**High-pH peptide prefractionation.** Dried peptide samples (TMT channels 1 to 4) were suspended in high-pH buffer (5 mM  $\text{NH}_4\text{OH}$ , pH 10.5), loaded onto an Agilent Zorbax Extend- $\text{C}_{18}$  column (3.5- $\mu\text{m}$  bead size, 300- $\text{\AA}$  pore size, 2.1 mm by 150 mm), and washed with buffer A (0.1% [vol/vol] formic acid, 2% [vol/vol] acetonitrile) for 10 min, followed by elution with an increasing gradient of buffer B (5 mM  $\text{NH}_4\text{OH}$ , 90% [vol/vol] acetonitrile). The gradient of buffer B was 3% to 30% for 55 min, then to 70% for 10 min, and finally to 90% for 5 min at a flow rate of 300  $\mu\text{l}/\text{minute}$ . Samples were collected every minute and pooled into 13 fractions, vacuum centrifuged, and then suspended in buffer A to a concentration of 0.1  $\mu\text{g}/\mu\text{l}$ .

**Mass spectrometry.** Samples were analyzed on a Q-Exactive mass spectrometer (ThermoFisher Scientific) coupled to an Easy-nLC1000 system (ThermoFisher Scientific, USA). Peptide samples were injected onto the liquid chromatography (LC) system using buffer A and were bound on a 75- $\mu\text{m}$  by 100-mm  $\text{C}_{18}$  Halo column (2.7- $\mu\text{m}$  bead size, 160- $\text{\AA}$  pore size). A flow rate of 300 nl/minute using an increasing linear gradient of buffer B (0.1% [vol/vol] formic acid, 99.9% [vol/vol] acetonitrile) was run from 1% to 30% for 110 min followed by 85% buffer B for 10 min. The mass spectrometer was operated in top-10 mode, with a full scan set at a resolution of 70,000 (at 400  $m/z$ ) across the  $m/z$  range of 350 to 1,850 (isolation window of 0.7  $m/z$ ), and an automatic gain control (AGC) target of 1e6 (or maximum fill time of 250 ms). Selected precursor ions were transferred from the C-trap to the higher energy collision dissociation (HCD) cell for fragmentation at a normalized collision energy of 35% with precursor dynamic exclusion of 90 s. Tandem mass spectrometry (MS/MS) spectra were collected at a resolution of 70,000 (at 200  $m/z$ ) with an AGC of 1e5, a maximum injection time of 250 ms, and a fixed first mass of 115.0  $m/z$ .

Raw files were exported to Proteome Discoverer v2.1 (ThermoFisher Scientific) for processing. Precursors selected for fragmentation that had greater than 30% interference were excluded from analysis. Methionine oxidation, N-terminal carbamylation, asparagine and glutamine deamidation, N-terminal acetylation, N-terminal glutamic acid to N-pyroglutamine, N-terminal glutamine to N-pyroglutamine, and TMT 10-plex labeling of primary amines were selected as dynamic modifications. Cysteine carbamidomethylation was designated a fixed modification. Minimum peptide length was set at 5. Spectra were searched against a custom *E. coli* C122 database that included the phage proteins, totaling 3,806 entries (Data Set S4). False-discovery rates were fixed at 1% at the peptide and protein level. Runs were normalized by dividing by all channels (e.g., 126, 128N) by the pooled control (128C),  $\log_2$  transformed, and further normalized by subtracting by the median of each sample group (Table S1). Sample infected 60<sub>1</sub> was excluded from statistical tests due to phage proteins being designated outliers by OutlierD quantile regression analysis (84). Host proteins lacking enough observations for quantitation at any time point or condition were not processed further. Student's *t* test was performed on the  $\log_2$ -transformed data. Due to effects of ratio compression and to appropriately control for false discovery in a (low-power) medium-scale experiment (85), significance was deemed with a protein fold change cutoff  $\geq \pm 1.5$ , *P* value  $< 0.025$ .

**RNA isolation and RNA-seq.** Biological triplicates of *E. coli* C122 were grown and infected with wild-type  $\phi\text{X174}$  at MOI=5. Phage infection was synchronized as for proteomics sampling. Following cell resuspension in 37°C LB medium, 5-ml samples were removed from infected and mock replicates at initial infection (time=0 min) and at 60 minutes after infection initiation. Samples were pelleted (3,500 RCF/5 min/4°C) and resuspended in 200  $\mu\text{l}$  1 $\times$  PBS, 400  $\mu\text{l}$  of RNeasy Protect Bacteria lysis reagent (Qiagen: 76506) was added, and the mixture was vortexed and incubated for 10 min at room temperature. Following protection, the RNeasy minikit (Qiagen; 74106) was used with the optional DNase step. RNA samples were then eluted, and RNA was quantified (Qubit RNA HS assay kit; ThermoFisher Scientific; Q32852) and stored at  $-80^\circ\text{C}$ . Sequencing library preparation was performed by Macrogen Inc. (South Korea). The rRNA from samples was depleted with a Ribo-Zero kit (Illumina), and the RNA library was generated with a TruSeq stranded mRNA kit for microbes. Libraries were sequenced with Illumina HiSeq 2500 (2  $\times$  100-bp mode). The PhiX control library was not used during the sequencing run to avoid cross-contamination.

Read quality was checked with FastQC followed by Rsubread analysis using the standard protocol (86). BAM files were processed with the Rsubread featureCount function against a manually generated General Feature Format (GFF2, or GTF) file derived from the [NZ\\_LT906474.1](#) RefSeq GFF3 file. RNA differential expression was analyzed using DESeq2 (87) and visualized using the ggplot2 R package (88). To analyze trends in differential expression, gene names were converted to UniProt identifiers using the Retrieve/ID mapping tool (89) and searched against the PANTHER database gene list analysis tool (90) using the statistical overrepresentation test against the internal reference *Escherichia coli* gene list to generate overrepresented GO terms for both cellular compartments and biological processes. The converted UniProt IDs were used to extract individual GO terms as before for all genes in the differentially expressed bins using the EcoCyc database (91).

**Databases and gene analysis.** *E. coli* C122 gene annotations for proteomics experiment and COG assignments were produced through the eggNOG-Mapper using default parameters (24). For  $\sigma^{32}$  and  $\sigma^{38}$  transcription factor assignments, we extracted orthologous gene members from the gold-standard *E. coli* K-12 gene annotations from the EcoCyc database (91) and assigned matching annotations to

C122 genes (Data Set S3). The PANTHER (25) database's statistical overrepresentation tests and functional classifications were used to map protein and transcript enrichments.

**Data availability.** Mass spectrometry proteomics data have been deposited to the ProteomeXchange Consortium via the PRIDE (92) partner repository with the data set identifier [PXD021681](https://doi.org/10.1093/ptm/10.1038/nrmicro.2017.61).

## SUPPLEMENTAL MATERIAL

Supplemental material is available online only.

**FIG S1**, EPS file, 1.6 MB.

**FIG S2**, EPS file, 1.1 MB.

**FIG S3**, EPS file, 1.8 MB.

**FIG S4**, PDF file, 1.1 MB.

**FIG S5**, PDF file, 2.3 MB.

**TABLE S1**, DOCX file, 0.02 MB.

**DATA SET S1**, XLSX file, 1.6 MB.

**DATA SET S2**, XLSX file, 0.6 MB.

**DATA SET S3**, XLSX file, 0.02 MB.

**DATA SET S4**, TXT file, 1.9 MB.

## ACKNOWLEDGMENTS

We recognize that this research was conducted on the traditional lands of the Wattamattagal clan of the Darug nation.

We thank Karthik Kamath, David Cantor, Sasha Tetu, and Varsha Naidu for assistance. Aspects of this research were conducted at the Australian Proteome Analysis Facility.

B.W.W. was supported by a Macquarie Research Excellence PhD Scholarship. P.R.J. was supported by NHMRC Ideas Grant APP118539 as well as the Molecular Sciences Department, Faculty of Science & Engineering, and the Deputy Vice-Chancellor (Research) of Macquarie University. D.Y.L. is a recipient of the Macquarie University Research Excellence PhD scholarship (MQRES) and CSIRO PhD Scholarship Program in Synthetic Biology (Synthetic Biology Future Science Platform).

The contributions of authors of this work according to the CRediT contribution taxonomy were as follows. B.W.W.: Conceptualization, Formal analysis, Investigation, Methodology, Visualization, Writing – Original draft, Writing – review & editing; D.Y.L.: Formal analysis, Investigation, Methodology, Visualization, Writing - original draft, Writing - review & editing; M.M.: Investigation, Methodology; D.P.: Formal analysis, Methodology; M. P.M.: Funding acquisition; Project administration; Resources; Supervision; Writing - review & editing. P.R.J.: Conceptualization; Formal analysis; Funding acquisition; Methodology; Project administration; Resources; Supervision; Writing - review & editing.

## REFERENCES

- Bondy-Denomy J, Pawluk A, Maxwell KL, Davidson AR. 2012. Bacteriophage genes that inactivate the CRISPR/Cas bacterial immune system. *Nature* 493:429–432. <https://doi.org/10.1038/nature11723>.
- De Smet J, Hendrix H, Blasdel BG, Danis-Wlodarczyk K, Lavigne R. 2017. *Pseudomonas* predators: understanding and exploiting phage-host interactions. *Nat Rev Microbiol* 15:517–530. <https://doi.org/10.1038/nrmicro.2017.61>.
- Zhao X, Chen C, Shen W, Huang G, Le S, Lu S, Li M, Zhao Y, Wang J, Rao X, Li G, Shen M, Guo K, Yang Y, Tan Y, Hu F. 2016. Global transcriptomic analysis of interactions between *Pseudomonas aeruginosa* and bacteriophage PaP3. *Sci Rep* 6:19237. <https://doi.org/10.1038/srep19237>.
- Chevallereau A, Blasdel BG, De Smet J, Monot M, Zimmermann M, Kogadeeva M, Sauer U, Jorth P, Whiteley M, Debarbieux L, Lavigne R. 2016. Next-generation “-omics” approaches reveal a massive alteration of host RNA metabolism during bacteriophage infection of *Pseudomonas aeruginosa*. *PLoS Genet* 12:e1006134. <https://doi.org/10.1371/journal.pgen.1006134>.
- Wei D, Zhang X. 2010. Proteomic analysis of interactions between a deep-sea thermophilic bacteriophage and its host at high temperature. *J Virol* 84:2365–2373. <https://doi.org/10.1128/JVI.01282-09>.
- Young JC, Dill BD, Pan C, Hettich RL, Banfield JF, Shah M, Fremaux C, Horvath P, Barrangou R, VerBerkmoes NC. 2012. Phage-induced expression of CRISPR-associated proteins is revealed by shotgun proteomics in *Streptococcus thermophilus*. *PLoS One* 7:e38077. <https://doi.org/10.1371/journal.pone.0038077>.
- Van den Bossche A, Ceysens PJ, De Smet J, Hendrix H, Bellon H, Leimer N, Wagemans J, Delattre AS, Cenens W, Aertsen A, Landuyt B, Minakhin L, Severinov K, Noben JP, Lavigne R. 2014. Systematic identification of hypothetical bacteriophage proteins targeting key protein complexes of *Pseudomonas aeruginosa*. *J Proteome Res* 13:4446–4456. <https://doi.org/10.1021/pr500796n>.
- Ceysens PJ, Minakhin L, Van den Bossche A, Yakunina M, Klimuk E, Blasdel B, De Smet J, Noben JP, Blasi U, Severinov K, Lavigne R. 2014. Development of giant bacteriophage PhiKZ is independent of the host transcription apparatus. *J Virol* 88:10501–10510. <https://doi.org/10.1128/JVI.01347-14>.
- Wu D, Yuan Y, Liu P, Wu Y, Gao M. 2014. Cellular responses in *Bacillus thuringiensis* CS33 during bacteriophage BTCS33 infection. *J Proteomics* 101:192–204. <https://doi.org/10.1016/j.jprot.2014.02.016>.
- Weintraub ST, Mohd Redzuan NH, Barton MK, Md Amin NA, Desmond MI, Adams LE, Ali B, Pardo S, Molleur D, Wu W, Newcomb WW, Osier MV, Black LW, Steven AC, Thomas JA. 2018. Global proteomic profiling of *Salmonella* infection by a giant phage. *J Virol* 93:e01833-18. <https://doi.org/10.1128/JVI.01833-18>.
- Lemay ML, Otto A, Maass S, Plate K, Becher D, Moineau S. 2019. Investigating *Lactococcus lactis* MG1363 response to phage p2 infection at the

- proteome level. *Mol Cell Proteomics* 18:704–714. <https://doi.org/10.1074/mcp.RA118.001135>.
12. Logel DY, Jaschke PR. 2020. A high-resolution map of bacteriophage  $\phi$ X174 transcription. *Virology* 547:47–56. <https://doi.org/10.1016/j.virol.2020.05.008>.
  13. Wright BW, Ruan J, Molloy MP, Jaschke PR. 2020. Genome modularization reveals overlapped gene topology is necessary for efficient viral reproduction. *ACS Synth Biol* 9:3079–3090. <https://doi.org/10.1021/acssynbio.0c00323>.
  14. Jaschke PR, Dotson GA, Hung KS, Liu D, Endy D. 2019. Definitive demonstration by synthesis of genome annotation completeness. *Proc Natl Acad Sci U S A* 116:24206–24213. <https://doi.org/10.1073/pnas.1905990116>.
  15. Jaschke PR, Lieberman EK, Rodriguez J, Sierra A, Endy D. 2012. A fully decompressed synthetic bacteriophage  $\phi$ X174 genome assembled and archived in yeast. *Virology* 434:278–284. <https://doi.org/10.1016/j.virol.2012.09.020>.
  16. Wichman HA, Millstein J, Bull JJ. 2005. Adaptive molecular evolution for 13,000 phage generations: a possible arms race. *Genetics* 170:19–31. <https://doi.org/10.1534/genetics.104.034488>.
  17. Hafenstein S, Fane BA. 2002.  $\phi$ X174 genome-capsid interactions influence the biophysical properties of the virion: evidence for a scaffolding-like function for the genome during the final stages of morphogenesis. *J Virol* 76:5350–5356. <https://doi.org/10.1128/jvi.76.11.5350-5356.2002>.
  18. Bernal RA, Hafenstein S, Esmeralda R, Fane BA, Rossmann MG. 2004. The  $\phi$ X174 protein J mediates DNA packaging and viral attachment to host cells. *J Mol Biol* 337:1109–1122. <https://doi.org/10.1016/j.jmb.2004.02.033>.
  19. Sun L, Young LN, Zhang X, Boudko SP, Fokine A, Zbornik E, Roznowski AP, Molineux IJ, Rossmann MG, Fane BA. 2014. Icosahedral bacteriophage  $\Phi$ X174 forms a tail for DNA transport during infection. *Nature* 505:432–435. <https://doi.org/10.1038/nature12816>.
  20. Sun Y, Roznowski AP, Tokuda JM, Klose T, Mauney A, Pollack L, Fane BA, Rossmann MG. 2017. Structural changes of tailless bacteriophage  $\Phi$ X174 during penetration of bacterial cell walls. *Proc Natl Acad Sci U S A* 114:13708–13713. <https://doi.org/10.1073/pnas.1716614114>.
  21. Shkoporov AN, Hill C. 2019. Bacteriophages of the human gut: the “known unknown” of the microbiome. *Cell Host Microbe* 25:195–209. <https://doi.org/10.1016/j.chom.2019.01.017>.
  22. Michel A, Clermont O, Denamur E, Tenaillon O. 2010. Bacteriophage  $\Phi$ X174’s ecological niche and the flexibility of its *Escherichia coli* lipopolysaccharide receptor. *Appl Environ Microbiol* 76:7310–7313. <https://doi.org/10.1128/AEM.02721-09>.
  23. Calderón-Celis F, Encinar JR, Sanz-Medel A. 2018. Standardization approaches in absolute quantitative proteomics with mass spectrometry. *Mass Spectrom Rev* 37:715–737. <https://doi.org/10.1002/mas.21542>.
  24. Huerta-Cepas J, Forslund K, Coelho LP, Szklarczyk D, Jensen LJ, von Mering C, Bork P. 2017. Fast genome-wide functional annotation through orthology assignment by eggNOG-Mapper. *Mol Biol Evol* 34:2115–2122. <https://doi.org/10.1093/molbev/msx148>.
  25. Mi H, Muruganujan A, Huang X, Ebert D, Mills C, Guo X, Thomas PD. 2019. Protocol update for large-scale genome and gene function analysis with the PANTHER classification system (v.14.0). *Nat Protoc* 14:703–721. <https://doi.org/10.1038/s41596-019-0128-8>.
  26. Lex A, Gehlenborg N, Strobel H, Vuilleumot R, Pfister H. 2014. UpSet: visualization of intersecting sets. *IEEE Trans Vis Comput Graph* 20:1983–1992. <https://doi.org/10.1109/TVCG.2014.2346248>.
  27. Sachelarü I, Winter L, Knyazev DG, Zimmermann M, Vogt A, Kuttner R, Ollinger N, Siligan C, Pohl P, Koch H-G. 2017. YidC and SecYEG form a heterotetrameric protein translocation channel. *Sci Rep* 7:101. <https://doi.org/10.1038/s41598-017-00109-8>.
  28. Komar J, Alvira S, Schulze RJ, Martin R, Nijeholt JALA, Lee SC, Dafforn TR, Deckers-Hebestreit G, Berger I, Schaffitzel C, Collinson I. 2016. Membrane protein insertion and assembly by the bacterial holo-translocon SecYEG-SecDF-YajC-YidC. *Biochem J* 473:3341–3354. <https://doi.org/10.1042/BCJ20160545>.
  29. Beckwith J. 2013. The Sec-dependent pathway. *Res Microbiol* 164:497–504. <https://doi.org/10.1016/j.resmic.2013.03.007>.
  30. Zuckert WR. 2014. Secretion of bacterial lipoproteins: through the cytoplasmic membrane, the periplasm and beyond. *Biochim Biophys Acta* 1843:1509–1516. <https://doi.org/10.1016/j.bbamcr.2014.04.022>.
  31. Kaplan E, Greene NP, Crow A, Koronakis V. 2018. Insights into bacterial lipoprotein trafficking from a structure of LolA bound to the LolC periplasmic domain. *Proc Natl Acad Sci U S A* 115:E7389–E7397. <https://doi.org/10.1073/pnas.1806822115>.
  32. Tanaka K, Matsuyama SI, Tokuda H. 2001. Deletion of *lolB*, encoding an outer membrane lipoprotein, is lethal for *Escherichia coli* and causes accumulation of lipoprotein localization intermediates in the periplasm. *J Bacteriol* 183:6538–6542. <https://doi.org/10.1128/JB.183.22.6538-6542.2001>.
  33. Mathelié-Guinlet M, Asmar AT, Collet J-F, Duffrène YF. 2020. Lipoprotein Lpp regulates the mechanical properties of the *E. coli* cell envelope. *Nat Commun* 11:1789. <https://doi.org/10.1038/s41467-020-15489-1>.
  34. Grabowicz M, Silhavy TJ. 2017. Redefining the essential trafficking pathway for outer membrane lipoproteins. *Proc Natl Acad Sci U S A* 114:4769–4774. <https://doi.org/10.1073/pnas.1702248114>.
  35. Cascales E, Bernadac A, Gavioli M, Lazzaroni J-C, Llobes R. 2002. Pal lipoprotein of *Escherichia coli* plays a major role in outer membrane integrity. *J Bacteriol* 184:754–759. <https://doi.org/10.1128/JB.184.3.754-759.2002>.
  36. Samsudin F, Ortiz-Suarez ML, Piggot TJ, Bond PJ, Khalid S. 2016. OmpA: a flexible clamp for bacterial cell wall attachment. *Structure* 24:2227–2235. <https://doi.org/10.1016/j.str.2016.10.009>.
  37. Bernhardt TG, Roof WD, Young R. 2000. Genetic evidence that the bacteriophage  $\phi$ X174 lysis protein inhibits cell wall synthesis. *Proc Natl Acad Sci U S A* 97:4297–4302. <https://doi.org/10.1073/pnas.97.8.4297>.
  38. Bernhardt TG, Struck DK, Young R. 2001. The lysis protein E of  $\phi$ X174 is a specific inhibitor of the *MraY*-catalyzed step in peptidoglycan synthesis. *J Biol Chem* 276:6093–6097. <https://doi.org/10.1074/jbc.M007638200>.
  39. Rodolis MT, Mihalyi A, O’Reilly A, Slikas J, Roper DI, Hancock REW, Bugg TDH. 2014. Identification of a novel inhibition site in translocase *MraY* based upon the site of interaction with lysis protein E from bacteriophage  $\phi$ X174. *Chembiochem* 15:1300–1308. <https://doi.org/10.1002/cbic.201402064>.
  40. Bouhss A, Trunkfield AE, Bugg TDH, Mengin-Lecreux D. 2008. The biosynthesis of peptidoglycan lipid-linked intermediates. *FEMS Microbiol Rev* 32:208–233. <https://doi.org/10.1111/j.1574-6976.2007.00089.x>.
  41. Witte A, Bläsi U, Halfmann G, Szostak M, Wanner G, Lubitz W. 1990.  $\Phi$ X174 protein E-mediated lysis of *Escherichia coli*. *Biochimie* 72:191–200. [https://doi.org/10.1016/0300-9084\(90\)90145-7](https://doi.org/10.1016/0300-9084(90)90145-7).
  42. Lubitz W, Halfmann G, Plapp R. 1984. Lysis of *Escherichia coli* after infection with  $\phi$ X174 depends on the regulation of the cellular autolytic system. *J Gen Microbiol* 130:1079–1087. <https://doi.org/10.1099/00221287-130-5-1079>.
  43. Bernhardt TG, Wang IN, Struck DK, Young R. 2002. Breaking free: “protein antibiotics” and phage lysis. *Res Microbiol* 153:493–501. [https://doi.org/10.1016/S0923-2508\(02\)01330-X](https://doi.org/10.1016/S0923-2508(02)01330-X).
  44. Doublet P, van Heijenoort J, Mengin-Lecreux D. 1992. Identification of the *Escherichia coli murl* gene, which is required for the biosynthesis of D-glutamic acid, a specific component of bacterial peptidoglycan. *J Bacteriol* 174:5772–5779. <https://doi.org/10.1128/jb.174.18.5772-5779.1992>.
  45. Gibbons HS, Kalb SR, Cotter RJ, Raetz CRH. 2005. Role of Mg<sup>2+</sup> and pH in the modification of *Salmonella* lipid A after endocytosis by macrophage tumour cells. *Mol Microbiol* 55:425–440. <https://doi.org/10.1111/j.1365-2958.2004.04409.x>.
  46. Huvet M, Toni T, Sheng X, Thorne T, Jovanovic G, Engl C, Buck M, Pinney JW, Stumpf MPH. 2011. The evolution of the phage shock protein response system: interplay between protein function, genomic organization, and system function. *Mol Biol Evol* 28:1141–1155. <https://doi.org/10.1093/molbev/msq301>.
  47. García LR, Molineux IJ. 1995. Incomplete entry of bacteriophage T7 DNA into T phage mid-containing *Escherichia coli*. *J Bacteriol* 177:4077–4083. <https://doi.org/10.1128/JB.177.14.4077-4083.1995>.
  48. Cheng X, Wang W, Molineux IJ. 2004. F exclusion of bacteriophage T7 occurs at the cell membrane. *Virology* 326:340–352. <https://doi.org/10.1016/j.virol.2004.06.001>.
  49. Dekoninck K, Létoquart J, Laguri C, Demange P, Bevernaegie R, Simorre J-P, Dehu O, Iorga BI, Elias B, Cho S-H, Collet J-F. 2020. Defining the function of OmpA in the Rcs stress response. *Elife* 9:e60861. <https://doi.org/10.7554/eLife.60861>.
  50. Wall E, Majdalani N, Gottesman S. 2018. The complex Rcs regulatory cascade. *Annu Rev Microbiol* 72:111–139. <https://doi.org/10.1146/annurev-micro-090817-062640>.
  51. Gaubig LC, Waldminghaus T, Narberhaus F. 2011. Multiple layers of control expression of the *Escherichia coli ibpAB* heat-shock operon. *Microbiology* 157:66–76. <https://doi.org/10.1099/mic.0.043802-0>.
  52. Lavigne R, Lecoutere E, Wagemans J, Cenens W, Aertens A, Schoofs L, Landuyt B, Paeshuyse J, Scheer M, Schobert M, Ceysens PJ. 2013. A multifaceted study of *Pseudomonas aeruginosa* shutdown by virulent podovirus LUZ19. *mBio* 4:e00061-13. <https://doi.org/10.1128/mBio.00061-13>.
  53. Mayol RF, Sinsheimer RL. 1970. Process of infection with bacteriophage  $\phi$ X174. XXXVI. Measurement of virus-specific proteins during a normal



- cycle of infection. *J Virol* 6:310–319. <https://doi.org/10.1128/JVI.6.3.310-319.1970>.
54. Mojardin L, Salas M. 2016. Global transcriptional analysis of virus-host interactions between phage  $\phi$ 29 and *Bacillus subtilis*. *J Virol* 90:9293–9304. <https://doi.org/10.1128/JVI.01245-16>.
  55. Fallico V, Ross RP, Fitzgerald GF, McAuliffe O. 2011. Genetic response to bacteriophage infection in *Lactococcus lactis* reveals a four-strand approach involving induction of membrane stress proteins, D-alanylation of the cell wall, maintenance of proton motive force, and energy conservation. *J Virol* 85:12032–12042. <https://doi.org/10.1128/JVI.00275-11>.
  56. Li G-W, Burkhardt D, Gross C, Weissman JS. 2014. Quantifying absolute protein synthesis rates reveals principles underlying allocation of cellular resources. *Cell* 157:624–635. <https://doi.org/10.1016/j.cell.2014.02.033>.
  57. Bernhardt TG, Roof WD, Young R. 2002. The *Escherichia coli* FKBP-type PPIase SlyD is required for the stabilization of the E lysis protein of bacteriophage  $\phi$ X174. *Mol Microbiol* 45:99–108. <https://doi.org/10.1046/j.1365-2958.2002.02984.x>.
  58. Porter NT, Hryckowian AJ, Merrill BD, Fuentes JJ, Gardner JO, Glowacki RWP, Singh S, Crawford RD, Snitkin ES, Sonnenburg JL, Martens EC. 2020. Phase-variable capsular polysaccharides and lipoproteins modify bacteriophage susceptibility in *Bacteroides thetaiotaomicron*. *Nat Microbiol* 5:1170–1181. <https://doi.org/10.1038/s41564-020-0746-5>.
  59. Poranen MM, Ravantti JJ, Grann AM, Gupta R, Auvinen P, Bamford DH. 2006. Global changes in cellular gene expression during bacteriophage PRD1 infection. *J Virol* 80:8081–8088. <https://doi.org/10.1128/JVI.00065-06>.
  60. Kamenšek S, Žgur-Bertok D. 2013. Global transcriptional responses to the bacteriocin colicin M in *Escherichia coli*. *BMC Microbiol* 13:42. <https://doi.org/10.1186/1471-2180-13-42>.
  61. Carra S, Alberti S, Arrigo PA, Benesch JL, Benjamin IJ, Boelens W, Bartelt-Kirbach B, Brundel B, Buchner J, Bukau B, Carver JA, Ecroyd H, Emanuelsson C, Finet S, Golenhofen N, Goloubinoff P, Gusev N, Haslbeck M, Hightower LE, Kampinga HH, Kleivt RE, Liberek K, Mchaourab HS, McMenimen KA, Poletti A, Quinlan R, Strelkov SV, Toth ME, Vierling E, Tanguay RM. 2017. The growing world of small heat shock proteins: from structure to functions. *Cell Stress Chaperones* 22:601–611. <https://doi.org/10.1007/s12192-017-0787-8>.
  62. Baneyx F, Mujacic M. 2004. Recombinant protein folding and misfolding in *Escherichia coli*. *Nat Biotechnol* 22:1399–1408. <https://doi.org/10.1038/nbt1029>.
  63. Mogk A, Bukau B, Kampinga HH. 2018. Cellular handling of protein aggregates by disaggregation machines. *Mol Cell* 69:214–226. <https://doi.org/10.1016/j.molcel.2018.01.004>.
  64. Mogk A, Ruger-Herreros C, Bukau B. 2019. Cellular functions and mechanisms of action of small heat shock proteins. *Annu Rev Microbiol* 73:89–110. <https://doi.org/10.1146/annurev-micro-020518-115515>.
  65. Ravantti JJ, Ruokoranta TM, Alapuranen AM, Bamford DH. 2008. Global transcriptional responses of *Pseudomonas aeruginosa* to phage PRR1 infection. *J Virol* 82:2324–2329. <https://doi.org/10.1128/JVI.01930-07>.
  66. Gill RT, Valdes JJ, Bentley WE. 2000. A comparative study of global stress gene regulation in response to overexpression of recombinant proteins in *Escherichia coli*. *Metab Eng* 2:178–189. <https://doi.org/10.1006/mben.2000.0148>.
  67. Lethanh H, Neubauer P, Hoffmann F. 2005. The small heat-shock proteins IbpA and IbpB reduce the stress load of recombinant *Escherichia coli* and delay degradation of inclusion bodies. *Microb Cell Fact* 4:6. <https://doi.org/10.1186/1475-2859-4-6>.
  68. Maaroufi H, Tanguay RM. 2013. Analysis and Phylogeny of small heat shock proteins from marine viruses and their cyanobacteria host. *PLoS One* 8:e81207. <https://doi.org/10.1371/journal.pone.0081207>.
  69. Chen L-X, Méheust R, Crits-Christoph A, McMahon KD, Nelson TC, Slater GF, Warren LA, Banfield JF. 2020. Large freshwater phages with the potential to augment aerobic methane oxidation. *Nat Microbiol* 5:1504–1515. <https://doi.org/10.1038/s41564-020-0779-9>.
  70. Perrody E, Cirinesi A-M, Desplats C, Keppel F, Schwager F, Tranier S, Georgopoulos C, Genevaux P. 2012. A bacteriophage-encoded J-domain protein interacts with the DnaK/Hsp70 chaperone and stabilizes the heat-shock factor  $\sigma$ 32 of *Escherichia coli*. *PLoS Genet* 8:e1003037. <https://doi.org/10.1371/journal.pgen.1003037>.
  71. Chamakura KR, Tran JS, Young R. 2017. MS2 lysis of *Escherichia coli* depends on host chaperone DnaJ. *J Bacteriol* 199:e00058-17. <https://doi.org/10.1128/JB.00058-17>.
  72. Zeilstra-Ryalls J, Fayet O, Baird L, Georgopoulos C. 1993. Sequence analysis and phenotypic characterization of groEL mutations that block lambda and T4 bacteriophage growth. *J Bacteriol* 175:1134–1143. <https://doi.org/10.1128/jb.175.4.1134-1143.1993>.
  73. Hanninen AL, Bamford DH, Bamford JK. 1997. Assembly of membrane-containing bacteriophage PRD1 is dependent on GroEL and GroES. *Virology* 227:207–210. <https://doi.org/10.1006/viro.1996.8308>.
  74. Ding Y, Duda RL, Hendrix RW, Rosenberg JM. 1995. Complexes between chaperonin GroEL and the capsid protein of bacteriophage HK97. *Biochemistry* 34:14918–14931. <https://doi.org/10.1021/bi00045a037>.
  75. Semenyuk PI, Moiseenko AV, Sokolova OS, Muronetz VI, Kurochkina LP. 2020. Structural and functional diversity of novel and known bacteriophage-encoded chaperonins. *Int J Biol Macromol* 157:544–552. <https://doi.org/10.1016/j.ijbiomac.2020.04.189>.
  76. Takano T, Kakefuda T. 1972. Involvement of a bacterial factor in morphogenesis of bacteriophage capsid. *Nat New Biol* 239:34–37. <https://doi.org/10.1038/newbio239034a0>.
  77. Young KD, Anderson RJ, Hafner RJ. 1989. Lysis of *Escherichia coli* by the bacteriophage phiX174 E protein: inhibition of lysis by heat shock proteins. *J Bacteriol* 171:4334–4341. <https://doi.org/10.1128/JB.171.8.4334-4341.1989>.
  78. Zhao L, Stancik AD, Brown CJ. 2012. Differential transcription of bacteriophage  $\phi$ X174 genes at 37°C and 42°C. *PLoS One* 7:e35909. <https://doi.org/10.1371/journal.pone.0035909>.
  79. Hecht A, Filliben J, Munro SA, Salit M. 2018. A minimum information standard for reproducing bench-scale bacterial cell growth and productivity. *Commun Biol* 1:219. <https://doi.org/10.1038/s42003-018-0220-6>.
  80. Rokyta DR, Abdo Z, Wichman HA. 2009. The genetics of adaptation for eight microvirid bacteriophages. *J Mol Evol* 69:229–239. <https://doi.org/10.1007/s00239-009-9267-9>.
  81. Fane BA, Hayashi M. 1991. Second-site suppressors of a cold-sensitive prohead accessory protein of bacteriophage phi X174. *Genetics* 128:663–671. <https://doi.org/10.1093/genetics/128.4.663>.
  82. Newbold JE, Sinsheimer RL. 1970. The process of infection with bacteriophage  $\phi$ X174: XXXII. Early steps in the infection process: attachment, eclipse and DNA penetration. *J Mol Biol* 49:49–66. [https://doi.org/10.1016/0022-2836\(70\)90375-X](https://doi.org/10.1016/0022-2836(70)90375-X).
  83. Rappsilber J, Mann M, Ishihama Y. 2007. Protocol for micro-purification, enrichment, pre-fractionation and storage of peptides for proteomics using StageTips. *Nat Protoc* 2:1896–1906. <https://doi.org/10.1038/nprot.2007.261>.
  84. Cho H, Kim YJ, Jung HJ, Lee SW, Lee JW. 2008. OutlierD: an R package for outlier detection using quantile regression on mass spectrometry data. *Bioinformatics* 24:882–884. <https://doi.org/10.1093/bioinformatics/btn012>.
  85. Pascovici D, Handler DC, Wu JX, Haynes PA. 2016. Multiple testing corrections in quantitative proteomics: a useful but blunt tool. *Proteomics* 16:2448–2453. <https://doi.org/10.1002/pmic.201600044>.
  86. Liao Y, Smyth GK, Shi W. 2019. The R package Rsubread is easier, faster, cheaper and better for alignment and quantification of RNA sequencing reads. *Nucleic Acids Res* 47:e47. <https://doi.org/10.1093/nar/gkz114>.
  87. Love MI, Huber W, Anders S. 2014. Moderated estimation of fold change and dispersion for RNA-seq data with DESeq2. *Genome Biol* 15:550. <https://doi.org/10.1186/s13059-014-0550-8>.
  88. Wickham H. 2016. ggplot2: elegant graphics for data analysis. Springer-Verlag, New York, NY. <https://ggplot2.tidyverse.org>.
  89. The UniProt Consortium. 2018. UniProt: the universal protein knowledgebase. *Nucleic Acids Res* 46:2699. <https://doi.org/10.1093/nar/gky092>.
  90. Thomas PD, Kejarawal A, Guo N, Mi H, Campbell MJ, Muruganujan A, Lazareva-Ulitsky B. 2006. Applications for protein sequence–function evolution data: mRNA/protein expression analysis and coding SNP scoring tools. *Nucleic Acids Res* 34:W645–W650. <https://doi.org/10.1093/nar/gkl229>.
  91. Keseler IM, Mackie A, Santos-Zavaleta A, Billington R, Bonavides-Martinez C, Caspi R, Fulcher C, Gama-Castro S, Kothari A, Krummenacker M, Latendresse M, Muniz-Rascado L, Ong Q, Paley S, Peralta-Gil M, Subhraveti P, Velazquez-Ramirez DA, Weaver D, Collado-Vides J, Paulsen I, Karp PD. 2017. The EcoCyc database: reflecting new knowledge about *Escherichia coli* K-12. *Nucleic Acids Res* 45:D543–D550. <https://doi.org/10.1093/nar/gkw1003>.
  92. Perez-Riverol Y, Csordas A, Bai J, Bernal-Llinares M, Hewapathirana S, Kundu DJ, Inuganti A, Griss J, Mayer G, Eisenacher M, Pérez E, Uszkoreit J, Pfeuffer J, Sachsenberg T, Yilmaz Ş, Tiwary S, Cox J, Audain E, Walzer M, Jarnuczak AF, Ternent T, Brazma A, Vizcaíno JA. 2019. The PRIDE database and related

- tools and resources in 2019: improving support for quantification data. *Nucleic Acids Res* 47:D442–D450. <https://doi.org/10.1093/nar/gky1106>.
93. Morán LT, Kityk R, Mayer MP, Rüdiger SGD. 2018. Hsp90 breaks the deadlock of the Hsp70 chaperone system. *Mol Cell* 70:545–552.e9. <https://doi.org/10.1016/j.molcel.2018.03.028>.
94. Moayed F, Bezrukavnikov S, Naqvi MM, Groitl B, Cremers CM, Kramer G, Ghosh K, Jakob U, Tans SJ. 2020. The anti-aggregation holdase Hsp33 promotes the formation of folded protein structures. *Biophys J* 118:85–95. <https://doi.org/10.1016/j.bpj.2019.10.040>.
95. Gamer J, Multhaup G, Tomoyasu T, McCarty JS, Rüdiger S, Schönfeld HJ, Schirra C, Bujard H, Bukau B. 1996. A cycle of binding and release of the DnaK, DnaJ and GrpE chaperones regulates activity of the *Escherichia coli* heat shock transcription factor sigma32. *EMBO J* 15:607–617. <https://doi.org/10.1002/j.1460-2075.1996.tb00393.x>.
96. Rohrwild M, Coux O, Huang HC, Moerschell RP, Yoo SJ, Seol JH, Chung CH, Goldberg AL. 1996. HslV-HslU: a novel ATP-dependent protease complex in *Escherichia coli* related to the eukaryotic proteasome. *Proc Natl Acad Sci U S A* 93:5808–5813. <https://doi.org/10.1073/pnas.93.12.5808>.